Available online at www.sciencedirect.com
ScienceDirect
Advances in Space Research 40 (2007) 1042–1048
ADVANCES IN SPACE RESEARCH (a COSPAR publication)
www.elsevier.com/locate/asr

Coronal mass ejections: Solar cycle aspects

Hebe Cremades [a,b,*], O.C. St. Cyr [b]

[a] NASA Postdoctoral Program, Greenbelt, MD 20771, United States of America
[b] NASA Goddard Space Flight Center, Mail Code 671, Greenbelt, MD 20771, United States of America

Received 22 November 2006; received in revised form 4 January 2007; accepted 26 January 2007

Abstract

Research in the area of coronal mass ejections (CMEs) is now mature, since their discovery coincided with the first coronagraph that was flown in space in 1971. However, the continuity of space coronagraphs and similar instruments has allowed the detection and measurement of CMEs over almost three consecutive solar cycles. Their importance in the space weather field is well established, and some researchers believe the phenomenon may also be important for the longer-term space climate studies. In this review, we summarize the solar cycle variation of the main properties of CMEs detected by previous and ongoing missions. These include rate of detection, apparent angular width, detected mass, apparent speed, and apparent latitude. Their behavior in time is presented and discussed.

Keywords: Sun; Coronal mass ejections (CMEs); Corona; Evolution

1. Introduction

Coronal Mass Ejections (CMEs) are enormous eruptions of plasma and magnetic fields ejected from the Sun into interplanetary space, seen by coronagraphs as they move out of their field of view over the course of minutes to hours. Since their brightness is of the order of magnitude of that of the solar corona, they can only be observed by blocking the intense glare of the photosphere by means of an occulting disc. Although total solar eclipse expeditions had been undertaken for more than a century, the short time scale (a few minutes) prevented the discovery of CMEs until the early 1970s, when coronagraphs were first put in space. Since then, several space missions have had among their goals the observation of these eruptions. Unfortunately, the time coverage of the solar corona has not been continuous, having several gaps that range from months to years.

The first coronagraph to fly on a spacecraft was built by the Naval Research Laboratory (NRL) and mounted on the Orbiting Solar Observatory-7 (OSO-7) NASA satellite (Koomen et al., 1975). It discovered its first CME, at the time dubbed a "coronal transient", on December 14, 1971 (Tousey, 1973). In total, this white-light coronagraph observed about two dozen CMEs during the period November 1971–May 1973. While OSO-7 was still operative, a coronagraph built by the High Altitude Observatory (HAO) flew on Skylab, as part of the Apollo Telescope Mount (ATM) suite of solar experiments (MacQueen et al., 1974). The latter had a smaller field of view (2–6 solar radii, vs. 3–10 Rs) but superior resolution and stray light characteristics. It observed ~100 CMEs from May 1973 to February 1974 (Hildner et al., 1976). By the end of 1974, Helios 1 was launched, followed by its twin Helios 2 in January 1976 (Schwenn and Marsch, 1990, 1991). They did not carry coronagraphs on board, but zodiacal light photometers, which were capable of detecting CMEs off the solar limb. Until 1985, they observed hundreds of CMEs in the inner heliosphere (Jackson, 1985). After an interlude of a few years without space-borne coronagraphs, the Solwind coronagraph, built by NRL as well, flew on Air Force Satellite P78-1. This longer-lasting mission (from March 1979 to September 1985) had similar characteristics as OSO-7 and recorded over 1500 CMEs (Sheeley et al., 1986). Shortly after Solwind's start, HAO's

* Corresponding author.
E-mail address: cremades@lssp-mail.gsfc.nasa.gov (H. Cremades).

0273-1177/$30
doi:10.1016/j.asr.2007.01.088

Coronagraph/Polarimeter got underway, onboard the Solar Maximum Mission (MacQueen et al., 1980). It operated from March to September 1980 and from June 1984 until November 1989, detecting with improved resolution in total ~1350 CMEs (Burkepile and St. Cyr, 1993). The White Light Coronagraph aboard the short SPARTAN Missions in April 1993, September 1995, and November 1998, respectively, contributed with brief observations (Fisher and Guhathakurta, 1994).

A new era for CME studies began with the Solar and Heliospheric Observatory (SOHO, Domingo et al., 1995), a joint ESA–NASA effort which is still in operation. Since its launch in December 1995, it has continuously observed the Sun for a full 11-year solar cycle, with only one major data gap in June–September 1998. Its cutting edge Large Angle Spectroscopic Coronagraph (LASCO; Brueckner et al., 1995) has detected over 10,000 CMEs (e.g., Yashiro et al., 2004), thanks to its superior stray light rejection, higher spatial resolution, improved dynamic range and temporal cadence. The Solar Mass Ejection Imager (Jackson et al., 2004), onboard the Coriolis spacecraft, can image practically the whole sky in white light, which enables it to track at least some CMEs in their journey away from the Sun (e.g., Tappin et al., 2004; Howard et al., 2006; Webb et al., 2006). Since the start of its mission, it has observed a few hundreds of CMEs across the sky.

At present, CMEs can also be observed from Earth, with the aid of the MK4 coronagraph at Mauna Loa Solar Observatory (Fisher et al., 1981). It has provided routine daily observations since October 1998. Its predecessor MK3 had successfully operated from 1980 until September 1999. Also ground-based, interplanetary scintillation (IPS) antennas are able to track some CMEs, via the principle of scintillation of radio sources due to electron density inhomogeneities in the solar wind (e.g., Manoharan, 2006).

The longest continuous survey of the solar corona by a single space-borne telescope has been provided by SOHO, located at the L1 Lagrangian point. Until then, and since the discovery of CMEs, the coverage had been intermittent. Previous space missions were orbiting Earth, and therefore, constrained to observe only during their dayside passage, and they had limited lifetimes. Ground-based coronagraphs are also limited by weather and the diurnal passage of the Sun at their location. For these reasons, the CME observation series is incomplete and affected by duty cycle variations. The available data that covers most of solar cycles 21–23 have been compiled and are presented in the next section.

2. Basic properties of CMEs

Past and ongoing space missions have increasingly contributed to our knowledge regarding CMEs. Putting together their data sets, it is possible to follow the main properties of CMEs for almost three solar cycles. This review is meant to be an update of previous assemblages of the basic CME properties, presented, e.g., in Webb and Howard (1994) and in St. Cyr et al. (1999).

2.1. CME detection rate

The detection rate refers to the ratio between the observed number of CMEs and the time span in days, during which those CMEs were detected. Fig. 1 displays the CME detection rate from the year 1973 until present, in comparison with the solar flux at 2800 MHz (or 10.7 cm). The latter data, adjusted to 1 AU, were collected at the Ottawa/Penticton station and are available at www.ngdc.noaa.gov. Even if sunspot number records extend over a much longer reference frame than solar radio flux measurements, they have been derived from multiple sources, requiring normalization due to the variety of observers. Therefore, we consider the 10.7 cm solar flux as a more reliable indicator of solar cycle evolution than sunspot number, since it is described by a unique, unambiguous number. Although their records have started relatively

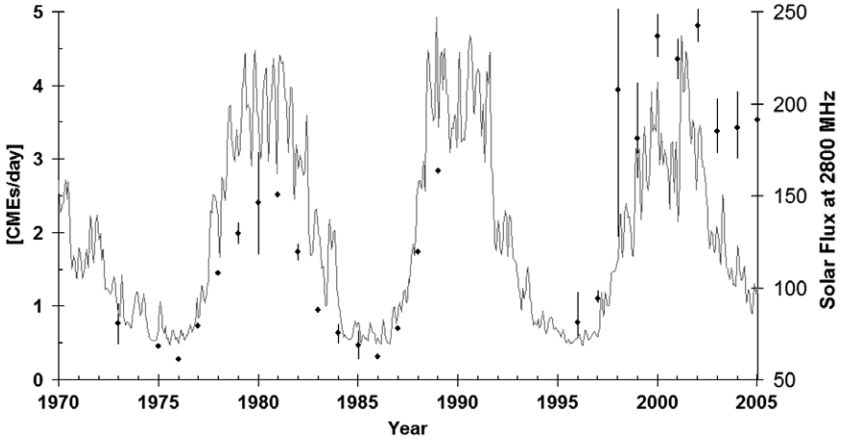

Fig. 1. Yearly CME rate of detection (black dots) in comparison with the solar flux at 2800 MHz (grey line). The values for different time periods correspond to various instruments. 1973: coronagraph on Skylab, 1975–1978: Helios' photometers, 1979 and 1981–1983: Solwind, 1980 and 1984–1989: coronagraph on SMM, 1996–2005: LASCO. After Webb and Howard (1994) and St. Cyr et al. (2000).

recently (6 decades ago), they extend long enough to cover the time interval in which CMEs have been observed. Fig. 1 covers almost three solar cycles, including solar cycles 21 (~1976–1985), 22 (~1986–1995) and 23 (~1996–2005). Most of solar cycle 22 lacks data points, since there were no space-borne coronagraphs during 1990–1995. CME rates for the years 1973–1989 are based in values from Webb and Howard (1994), which had been adjusted by those authors for duty cycles and visibility functions. They include data from coronagraphs on Skylab, P-78 and SMM, as well as from the Helios's photometers. CME rates for the SOHO years have been calculated from the LASCO CME Catalog at www://cdaw.gsfc.nasa.gov/CME_list/. Error bars in the figure have been calculated according to the logic applied by St. Cyr et al. (2000): the lower error bars represent the CME rate obtained if no CMEs occur within the data gaps, that is, without duty cycle correction. On the other hand, the upper bars assume that a maximum number of CMEs has occurred during LASCO C2 data gaps longer than 3 h. The assumed maximum has been determined using the maximum number of CMEs occurring in one day during each of 12 months, in order to obtain yearly averages of this maximum. Large upper limits may thus be an effect produced by exceptional days of high solar activity.

The CME rate in Fig. 1 clearly follows the solar cycle, independently of the instrument used. However, it also was apparently larger in cycle 23 versus cycle 21, in spite of having been corrected for duty cycle. During the years of maximum activity of solar cycle 21, the average CME rate was of about 2 per day, while for solar cycle 23, it increased to about 4 per day. Likewise, during minimum activity of solar cycles 21 and 22 the average CME rate lied near 0.25 CMEs/day, while for solar cycle 23 it reached the 0.75 CMEs/day. An apparent reason for this behavior is the superior performance (i.e., reduced levels of stray light present) in the LASCO coronagraphs, in comparison with their predecessors. The LASCO CME occurrence rate presented by Gopalswamy (2004), comprising the years 1996–2003, shows similar rates in the minimum of solar cycle 23, but they reach 6 CMEs per day in the year 2002. Note however that the latter rate had not been duty-cycle corrected and was averaged over periods of one Carrington rotation, in contrast to the rate presented here, averaged over periods of one year. Another distinctive feature in Fig. 1 is that solar cycle 21 shows a smooth increase of activity, with a single-peak maximum. However, the SOHO years reveal a much sharper increase of activity in 1998. It must be taken into account that the values for this year are the most uncertain ones, due to two large data gaps that account for almost 6 months. The years 2004 and 2005 do not show so far a decline in the CME production, despite the quick decrease in solar activity. During the maximum of solar cycle 23, the CME rate exhibits two peaks, one in 2000 and a second in 2002, apparently coincident with the 10.7 cm solar flux peaks. This behavior of solar cycle maxima had been recognized a few decades ago (Gnevyshev, 1963). This was also discussed by Gopalswamy (2004), who in addition compares the location of the two peaks in both CME rate and sunspot number averaged over Carrington rotation periods.

2.2. CME apparent angular width

The angular width of CMEs typically refers to their projected, apparent span, in degrees. Unfortunately, the real value is usually unknown, due to Thomson scattering and to the two-dimensional nature of coronagraphic images. The best estimate of a CME's angular width can be obtained if it originates near the limb and thus propagates in the plane of the sky. Even in this case, which is the most favorable one, there remains a distribution of widths, ranging from ~5° to ~120° (Burkepile et al., 2004). Moreover, there is no information about the angular width in the direction of the line-of-sight. Determining the three-dimensional nature of CMEs is a primary goal of the recently launched Solar Terrestrial Relations Observatory (STEREO). The yearly averages in time, as deduced from

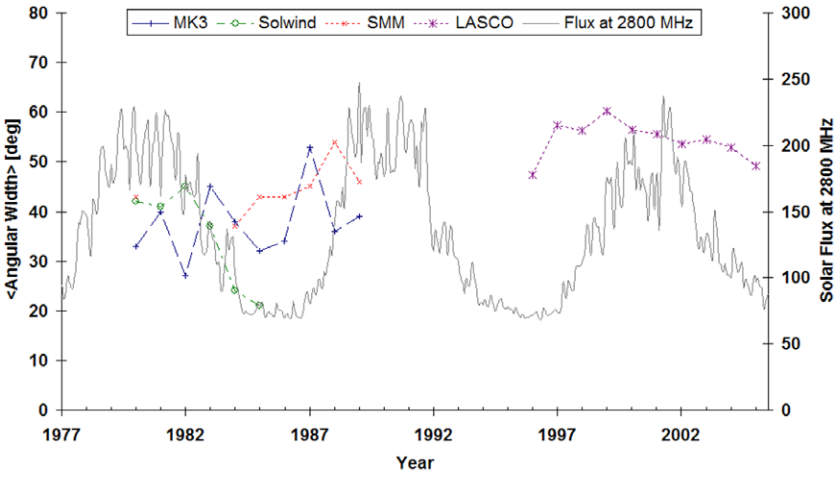

Fig. 2. Variation in time of the yearly averages of angular width as calculated from various sets of coronagraph data (dashed lines, see inset for details), in comparison with the solar flux at 2800 MHz (grey line). Values 1979–1989 were obtained from St. Cyr et al. (1999).

the measurements of various coronagraphs, are presented in Fig. 2. These are based on data from MK3, Solwind, and SMM, presented by St. Cyr et al. (1999); as well as data from LASCO, obtained from the LASCO CME Catalog. Following the convention adopted by Yashiro et al. (2004), only those events wider than 20° and narrower than 120° have been taken into account for the analysis of LASCO CME angular width. Narrow events could be associated with trailing material behind CMEs, as well as with streamer swelling. On the other hand, wide events are most likely the result of the projection of events traveling out of the plane of the sky, and would not give information on the real angular width of a CME. In this way, average values of angular width found for the LASCO dataset are identical to those presented by Yashiro et al. (2004) for the years 1996–2002. However, the criterion of angular width >20° and <120° leaves out those explosive events occurring at the solar limb, whose angular width is in reality over 120°, and also deflections of preexisting structures due to shock waves seen as "amber waves of grain" (Sheeley et al., 2000).

In general, MK3, SMM, and LASCO CME angular widths do not show significant correlation with the solar cycle. These datasets indicate merely a slight increasing trend during the rising phase of the solar cycle; however, the angular widths deduced from Solwind data appear to follow the solar cycle. In general, LASCO yearly average widths (ranging from 47° to 60° considering only CMEs with widths >20° and <120°) are larger than those of its predecessors (21–54°; these average values do include narrow and wide CMEs). This effect seems to be related to the improved performance of the LASCO coronagraphs with respect to previous missions: even the very faint and wider CMEs traveling out of the plane of the sky can be detected.

2.3. CME mass

The mass of a CME can be deduced from its excess brightness, after defining an assumed volume in which the CME is contained. The excess brightness of a CME is obtained by subtracting a pre-event image, and converting to units of mass (grams/pixel). Next, the area of interest is defined, for automated procedures usually an angular sector of the image that includes the span of the CME. Typical values of LASCO CME mass range from $\sim 5 \times 10^{14}$ to $\sim 5 \times 10^{16}$ g (Vourlidas et al., 2002). Fig. 3 exhibits the annual average mass, deduced from the mass values available in the LASCO CME Catalog. Again, only CMEs with angular widths between 20° and 120° have been considered, due to uncertainties in the mass determination for the remainder population. When contrasted with the solar flux at 2800 MHz, no obvious solar cycle dependence can be observed during the 9 years of SOHO data. Mass values calculated by Vourlidas (private communication) yield similar statistics. It was also the case for Solwind (Webb and Howard, 1994) and SMM CMEs (Hundhausen et al., 1994a), which show somewhat steady averages around

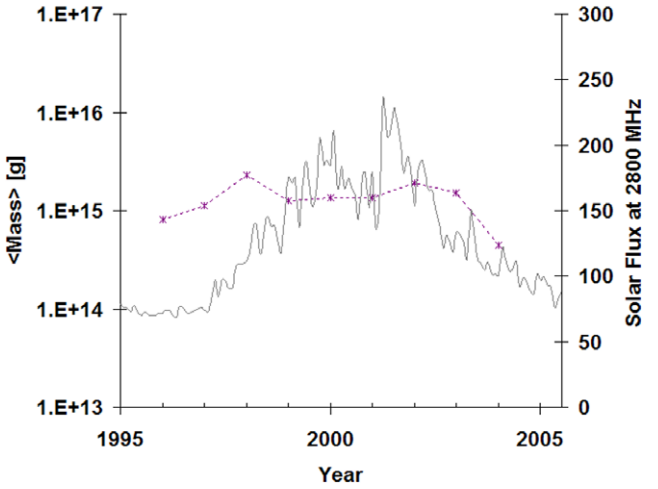

Fig. 3. Yearly average mass of LASCO CMEs vs. time (dashed line) and solar flux at 2800 MHz (grey line).

$2.5–4 \times 10^{15}$ g over several years of observations. The SOHO averages, though quite stable in time as well, are approximately lower by a factor of two. A plausible explanation is that SOHO, thanks to its improved dynamic range, is able to observe a vast amount of less massive CMEs, which may have traveled unnoticed in previous coronagraphs (Gopalswamy, 2004).

2.4. CME apparent speed

The speeds of CMEs are obtained by fitting measurements of the apparent height of a morphological feature (usually the leading edge) at different times – a height–time diagram. Typically height–time curves conform to linear motion, and their values can range from ~ 100 km s^{-1} to 2500 km s^{-1} or more. Most CME speeds are fairly constant above a few solar radii, but when measurements are available low in the corona, they commonly show acceleration in their initial phase. Therefore, in these cases the speed should be determined through second order or higher fits. As with the angular width, the CME speed is also subject to projection effects. The best conditions to obtain reliable values of CME speed are given if the ejecta is traveling in the plane of the sky, i.e., it originated near the solar limb. The farther the propagation direction is from the sky-plane, the smaller the radial speed component, and the larger the expansion speed, yet there seems to be a direct relationship between them (Dal Lago et al., 2003). Therefore, projected values of CME speed constitute a lower threshold.

In the comparison of CME speeds along time presented in Fig. 4, averages deduced by St. Cyr et al. (1999) are combined with up-to-date LASCO average speeds. For the latter, all the population of CMEs have been taken into account, without any distinction of their width. That is because even if wide CMEs are likely to have inherent projection effects attached, their speeds are nevertheless remarkably higher than for "normal"

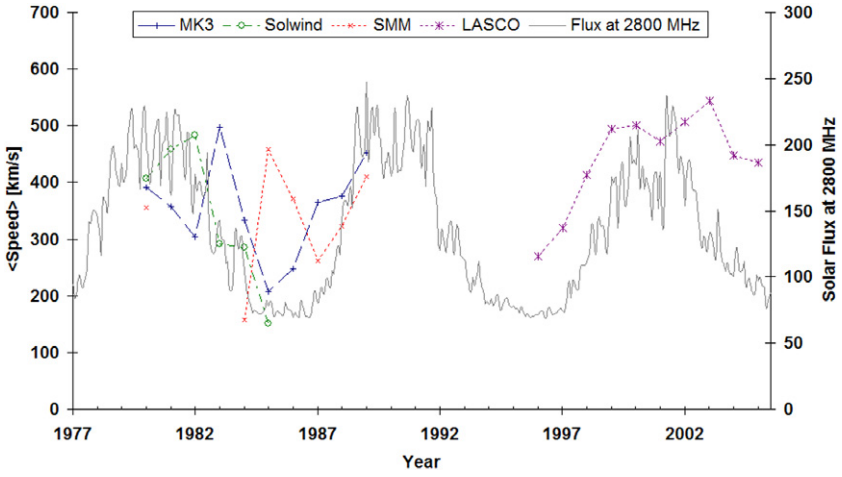

Fig. 4. Time variation of the yearly averaged CME speeds deduced from data of several coronagraphs (dashed lines, see inset for details), in comparison with the solar flux at 2800 MHz (grey line). Values 1979–1989 were obtained from St. Cyr et al. (1999).

CMEs, and should therefore be considered. From Fig. 4, a close relationship between the solar cycle and the speeds from Solwind CMEs is evident. MK3 shows a trough before the descending phase of the cycle, but also correspondence especially in solar minimum, reaching an annual average of 210 km s^{-1} in 1985. On the contrary, SMM speeds peaked at 460 km s^{-1} during the years of solar minimum (Hundhausen et al., 1994b). The discrepancy seen for the years 1985 and 1986 could be due to the small sample of SMM CMEs for which the speeds could be in fact deduced. Speeds of LASCO CMEs closely follow solar cycle 23, except for its second peak, which takes place in 2003 instead of 2002 and reaches 544 km s^{-1}. The average speed during the years of maximum activity, 2000–2002, is of 495 km s^{-1}. A decrease in the years 2004 and 2005 is already evident. The correspondence between speeds and the solar cycle has been previously reported for LASCO datasets (Yashiro et al., 2004; Gopalswamy, 2004).

2.5. CME apparent location

Due to the same constrains that two-dimensional images impose on the previously described CME properties, the CME location is an apparent magnitude as well. For instance, CMEs observed at polar locations can be seen as such just due to projection effects. The location of a feature in the corona is commonly expressed in terms of position angle (PA), i.e., the angle measured counterclockwise from the solar North. The most extensively used measurement is the central position angle, defined as the midpoint of the apparent width of the CME. However, when it is desired to compare this attribute with features at the solar surface, it becomes useful to convert position angle to apparent heliographic latitude (Hundhausen, 1993). Fig. 5 depicts the behavior in time of the RMS value of the latter quantity, in comparison with the 2800 MHz solar flux. Once more, MK3, Solwind, and SMM values have been obtained from St. Cyr et al. (1999); while SOHO val-

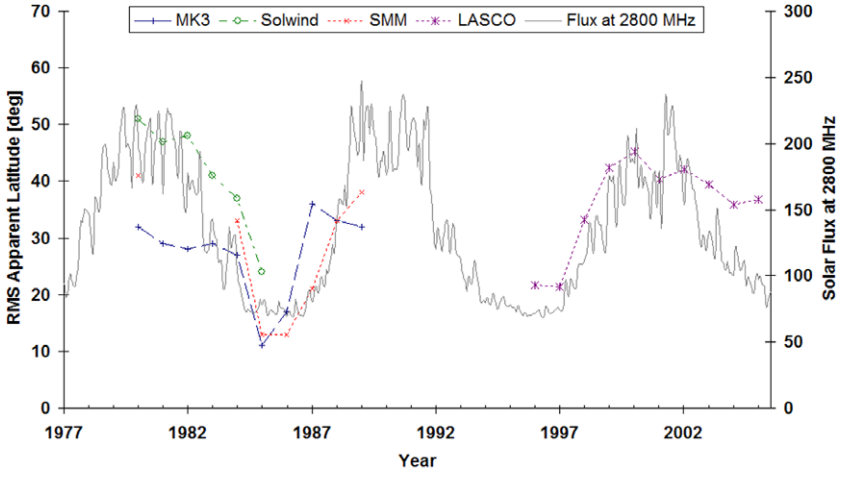

Fig. 5. RMS value of the apparent CME latitude vs. time (dashed lines, see inset for details), and solar flux at 2800 MHz (grey line).). Values 1979–1989 were obtained from St. Cyr et al. (1999).

ues have been deduced from the LASCO CME Catalog. All datasets exhibit a good correlation with the solar cycle curve: at times of solar minimum, CMEs tend to occur at low latitudes, while during solar maximum their average location moves towards much higher values, of ~40°. The same behavior has been reported by, e.g., Hundhausen (1993) for SMM CMEs, Howard et al. (1985, 1986) for Solwind events, St. Cyr et al. (1999) for MK3, and Yashiro et al. (2004) for LASCO CMEs. There is another remarkable recurring characteristic of the apparent latitudes, not evident in Fig. 5, but demonstrated in the above mentioned studies. The distributions of apparent latitude remain localized at low latitudes during solar minimum, while during solar maximum CME latitudes are broadly distributed, reaching polar latitudes. Their latitudes match well the locations of coronal streamers, which also show a strong cycle dependence. At solar minimum, the heliospheric current sheet is roughly aligned with the ecliptic plane, while during maximum activity it can be even found at polar regions, due to the restructuring of the global solar magnetic field. CME source regions in general, seem to be confined to ±30° during solar minimum, reaching high latitudes towards the maximum (Gopalswamy et al., 2003). However, when sorting CME source regions in two classes, they evolve differently in time. Those associated with active regions follow the butterfly diagram, thus appearing at lower latitudes as the cycle progresses. On the other hand, CME sources related to filaments outside active regions migrate towards higher latitudes, as noted by Gopalswamy (2004) and Cremades et al. (2006).

3. Summary and discussion

We have presented a survey over years of routinely collected data on CMEs (1980–2005), including Solwind, MK3, SMM, and LASCO. Their basic properties have been contrasted over three consecutive solar cycles, revealing correlations in some cases, and invariability over time in others. The CME rate shows a strong cycle dependence, though the counts are much higher for the SOHO era, most likely due to the enhanced performance of the LASCO coronagraphs. On the other hand, the evolution in time of the CME angular width and the CME mass do not exhibit a significant variation with the solar cycle. The fact that angular width and masses remain nearly constant over time would indicate that the CME phenomenon does not vary considerably, despite the important changes of emerging flux along the solar cycle. CMEs thus represent a "unit" of change in the large-scale structure of the Sun's outermost atmosphere. The CME speeds, however, do seem to depend on this cyclic changes. The sole exception is the SMM dataset, probably biased towards high values during solar minimum due to the small amount of sampled CMEs. The comparison between the solar-cycle dependent speeds, and the invariable angular width yields no correlation (Hundhausen et al., 1994b), thus corroborating their distinct nature. A further characteristic of CMEs that shows strong correspondence with the solar cycle is their location. It matches well with the location of coronal streamers, again shaped by the configuration of the global solar magnetic field at a specific time of the cycle.

Unfortunately, the mentioned properties may be, in many cases, subject of considerable projection effects. In order to reduce uncertainties in this statistical analysis of such apparent quantities, it is crucial to obtain an uncontaminated sample made up only of CMEs traveling in the plane of the sky (see study by Burkepile et al. (2004) for SMM CMEs). The ultimate way of doing it, would consist either in identifying the source regions of all CMEs to find those originating near the limb, or in deducing their true propagation direction from multipoint observations. The latter technique will be finally possible thanks to the recently launched STEREO Mission.

Since CME research is a relatively new field in solar physics, the variability of CME properties over time remains scarcely explored. Moreover, since CMEs are the primary cause of non-recurrent geomagnetic storms, understanding this phenomenon has become important to the space weather community, which is concerned with societal impacts of solar variability. To fully understand CMEs, it is crucial to ensure the continuity of space missions that continuously monitor the solar corona.

Acknowledgements

This research was supported in part by an appointment to the NASA Postdoctoral Program at the Goddard Space Flight Center, administered by Oak Ridge Associated Universities through a contract with NASA. The CME catalog is generated and maintained at the CDAW Data Center by NASA and The Catholic University of America in cooperation with the Naval Research Laboratory. SOHO is a project of international cooperation between ESA and NASA. The authors are thankful to S. Yashiro, who provided information on LASCO/C2 data gaps. H. Cremades thank Georgeta Maris, Marilena Mierla, and Kalevi Mursula, who made this contribution possible.

References

Brueckner, G.E., Howard, R.A., Koomen, M.J., Korendyke, C.M., Michels, D.J., Moses, J.D., Socker, D.G., Dere, K.P., Lamy, P.L., Llebaria, A., Bout, M.V., Schwenn, R., Simnett, G.M., Bedford, D.K., Eyles, C.J. The large angle spectroscopic coronagraph (LASCO). Sol. Phys. 162, 357–402, 1995.

Burkepile, J.T., St. Cyr, O.C. A revised and expanded catalogue of mass ejections observed by the Solar Maximum Mission coronagraph. NASA STI/Recon Technical Report N93-26556, Boulder, 1993.

Burkepile, J.T., Hundhausen, A.J., Stanger, A.L., St. Cyr, O.C., Seiden, J.A. Role of projection effects on solar coronal mass ejection properties: 1. A study of CMEs associated with limb activity. J. Geophys. Res. 109, A03103, doi:10.1029/2003JA01014, 2004.

Cremades, H., Bothmer, V., Tripathi, D. Properties of structured coronal mass ejections in solar cycle 23. Adv. Space Res. 38 (3), 461–465, 2006.

Dal Lago, A., Schwenn, R., Gonzalez, W.D. Relation between the radial speed and the expansion speed of coronal mass ejections. Adv. Space Res. 32, 2637–2640, 2003.

Domingo, V., Fleck, B., Poland, A.I. The SOHO mission: An overview. Sol. Phys. 162, 1–37, 1995.

Fisher, R.R., Guhathakurta, M. SPARTAN 201 White light coronagraph experiment. Space Sci. Rev. 170, 267–272, 1994.

Fisher, R.R., Lee, R.H., MacQueen, R.M., Poland, A.I. New Mauna Loa coronagraph systems. Appl. Opt. 20, 1094–1101, 1981.

Gnevyshev, M.N. The Corona and the 11-year cycle of solar activity. Soviet Astronomy 7, 311–318, 1963.

Gopalswamy, N., Lara, A., Yashiro, S., Nunes, S., Howard, R.A. Coronal mass ejection activity during solar cycle 23, in: A. Wilson (Ed.), Solar Variability as an Input to the Earth's Environment. ESA SP-535, pp. 403–414, 2003.

Gopalswamy, N. A global picture of CMEs in the inner heliosphere, in: Poletto, G., Suess, S.T. (Eds.), The Sun and the Heliosphere as an Integrated System. Kluwer, Dordrecht, pp. 201–251, 2004.

Hildner, E., Gosling, J.T., MacQueen, R.M., Munro, R.H., Poland, A.I., Ross, C.L. Frequency of coronal transients and solar activity. Sol. Phys. 48, 127–135, 1976.

Howard, R.A., Sheeley, N.R., Michels, D.J., Koomen, M.J. Coronal mass ejections – 1979–1981. J. Geophys. Res. 90, 8173–8191, 1985.

Howard, R.A., Sheeley, N.R., Michels, D.J., Koomen, M.J. The solar cycle dependence of coronal mass ejections, in: ASSL vol. 123: The Sun and the Heliosphere in Three Dimensions. Reidel Publishing Co. Dordrecht, pp. 107–111, 1986.

Howard, T.A., Webb, D.F., Tappin, S.J., Mizuno, D.R., Johnston, J.C. Tracking halo coronal mass ejections from 0-1 AU and space weather forecasting using the Solar Mass Ejection Imager (SMEI). J. Geophys. Res. 111 (4), A04105, doi:10.1029/2005JA01134, 2006.

Hundhausen, A.J. Sizes and locations of coronal mass ejections – SMM observations from 1980 and 1984–1989. J. Geophys. Res. 98, 13177–13200, 1993.

Hundhausen, A.J., Stanger, A.L., Serbicki, S.A. Mass and energy contents of coronal mass ejections: SMM results from 1980 and 1984–1988, in: J.J. Hunt (Ed.), Solar Dynamic Phenomena and Solar Wind Consequences, Proceedings of the Third SOHO Workshop. ESA SP-373, pp. 409–412, 1994a.

Hundhausen, A.J., Burkepile, J.T., St. Cyr, O.C. Speeds of coronal mass ejections: SMM observations from 1980 and 1984–1989. J. Geophys. Res. 99, 6543–6552, 1994b.

Jackson, B.V. Imaging of coronal mass ejections by the HELIOS spacecraft. Solar Phys. 100, 563–574, 1985.

Jackson, B.V., Buffington, A., Hick, P.P., et al. The solar mass-ejection imager (SMEI) Mission. Sol. Phys. 225, 177–207, 2004.

Koomen, M.J., Detwiler, C.R., Brueckner, G.E., Cooper, H.W., Tousey, R. White light coronagraph in OSO-7. Appl. Opt. 14 (3), 743–751, 1975.

MacQueen, R.M., Gosling, J.T., Hildner, E., Munro, R.H., Poland, A.I., Ross, C.L. The high altitude observatory white light coronagraph experiment, in: Newkirk, G. Jr. (Ed.), Coronal Disturbances. IAU, Reidel Publishing Co., Dordrecht, pp. 505–506, 1974.

MacQueen, R.M., Csoeke-Poeckh, A., Hildner, E., House, L., Reynolds, R., Stanger, A., Tepoel, H., Wagner, W. The high altitude observatory coronagraph/polarimeter on the solar maximum mission. Solar Phys. 65, 91–107, 1980.

Manoharan, P.K. Evolution of coronal mass ejections in the inner heliosphere: A study using white-light and scintillation images. Solar Phys. 235 (1–2), 345–368, 2006.

Schwenn, R., Marsch, E. Physics of the Inner Heliosphere I. Large-scale Phenomena. Springer Verlag, Berlin Heidelberg, 1990.

Schwenn, R., Marsch, E. Physics of the Inner Heliosphere II. Particles, Waves and Turbulence. Springer Verlag, Berlin Heidelberg, 1991.

Sheeley, N.R., Howard, R.A., Koomen, M.J., Michels, D.J. SOLWIND observations of coronal mass ejections during 1979–1985, in Solar flares and coronal physics using P/OF as a research tool. NASA Marshall Space Flight Center, 241–256, 1986.

Sheeley, N.R., Hakala, W.N., Wang, Y.-M. Detection of coronal mass ejection associated shock waves in the outer corona. J. Geophys. Res. 105 (A3), 5081–5092, 2000.

St. Cyr, O.C., Burkepile, J.T., Hundhausen, A.J., Lecinski, A.R. A comparison of ground-based and spacecraft observations of coronal mass ejections from 1980–1989. J. Geophys. Res. 104 (A6), 12493–12506, 1999.

St. Cyr, O.C., Howard, R.A., Sheeley, N.R., et al. Properties of coronal mass ejections: SOHO LASCO observations from January 1996 to June 1998. J. Geophys. Res. 105 (A8), 18169–18185, 2000.

Tappin, S.J., Buffington, A., Cooke, M.P., et al. Tracking a major interplanetary disturbance with SMEI. Geophys. Res. Lett. 31, L02802, doi:10.1029/2003GL01876, 2004.

Tousey, R. The Solar Corona. Space Res. 13 (2), 713–730, 1973.

Vourlidas, A., Buzasi, D., Howard, R.A., Esfandiari, E. Mass and energy properties of LASCO CMEs, in: A. Wilson (Ed.), Solar variability: from core to outer frontiers. The 10th European Solar Physics Meeting. ESA Publications Division SP-506, 1, pp. 91–94, 2002.

Webb, D.F., Howard, R.A. The solar cycle variation of coronal mass ejections and the solar wind mass flux. J. Geophys. Res. 99 (A3), 4201–4220, 1994.

Webb, D.F., Mizuno, D.R., Buffington, A., et al. Solar Mass Ejection Imager (SMEI) observations of coronal mass ejections (CMEs) in the heliosphere. J. Geophys. Res. 111, A12101, doi:10.1029/2006JA01165, 2006.

Yashiro, S., Gopalswamy, N., Michalek, G., St. Cyr, O.C., Plunkett, S.P., Rich, N.B., Howard, R.A. A catalog of white light coronal mass ejections observed by the SOHO spacecraft. J. Geophys. Res., A07105, doi:10.1029/2003JA01028, 2004.